

Support Information

Multi-networked nanofibrous aerogel supported by heterojunction photocatalysts with excellent dispersion and stability for photocatalysis

Jinli Qiu^a, Pei Fan^a, Cailiang Yue^a, Fuqiang Liu^{*a, b}, Aimin Li^{a, b}

^a State Key Laboratory of Pollution Control and Resources Reuse, School of the Environment, Nanjing University, Nanjing 210023, P.R. China

^b State Environmental Protection Engineering Center for Organic Chemical Industrial Waste Water Disposal Resource Reuse, Nanjing 210023, P. R. China

*Corresponding author. Tel: +86 13913871032.
E-mail address: lfq@nju.edu.cn (Fuqiang Liu)

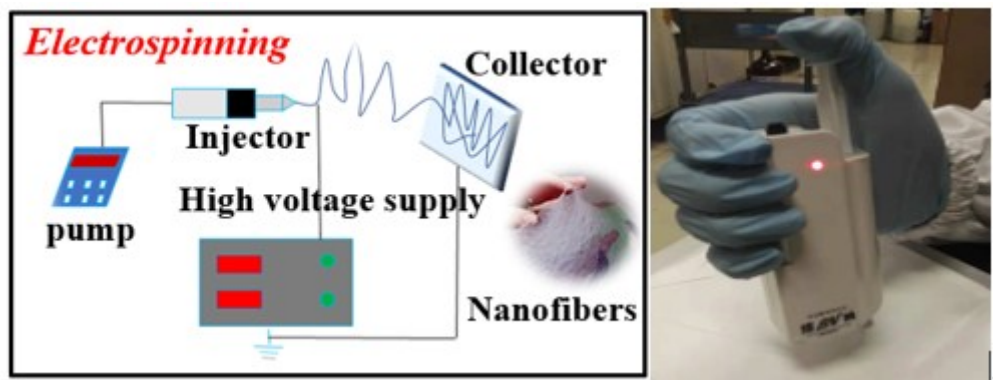


Figure S1. The schematic diagram of electrospinning process for PAN nanofibers.

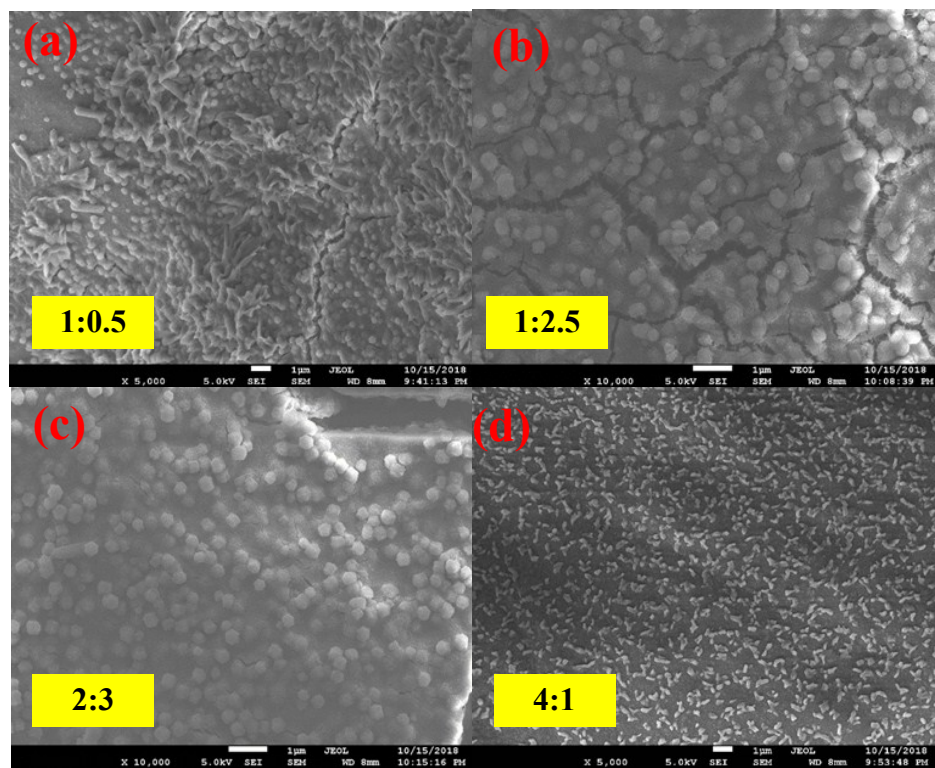


Figure S2. The SEM images of NM88 with different mass ratio of Fe (III) and linkers.

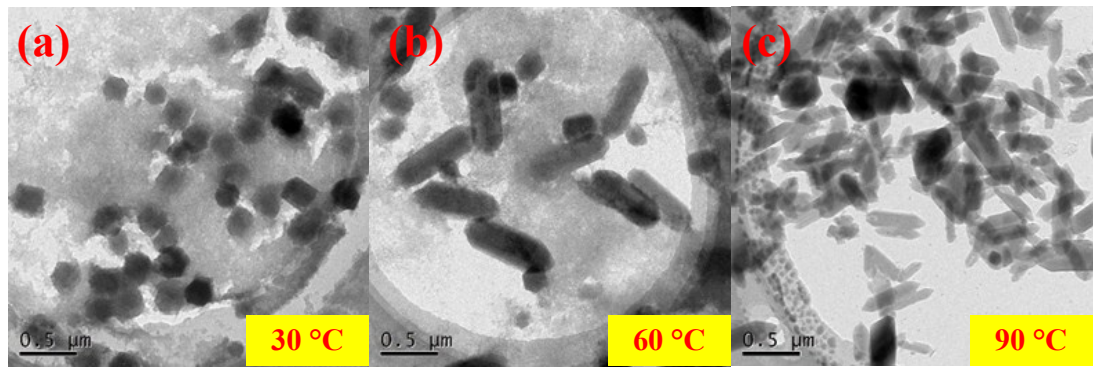


Figure S3. The TEM images of NM88 under different temperatures.

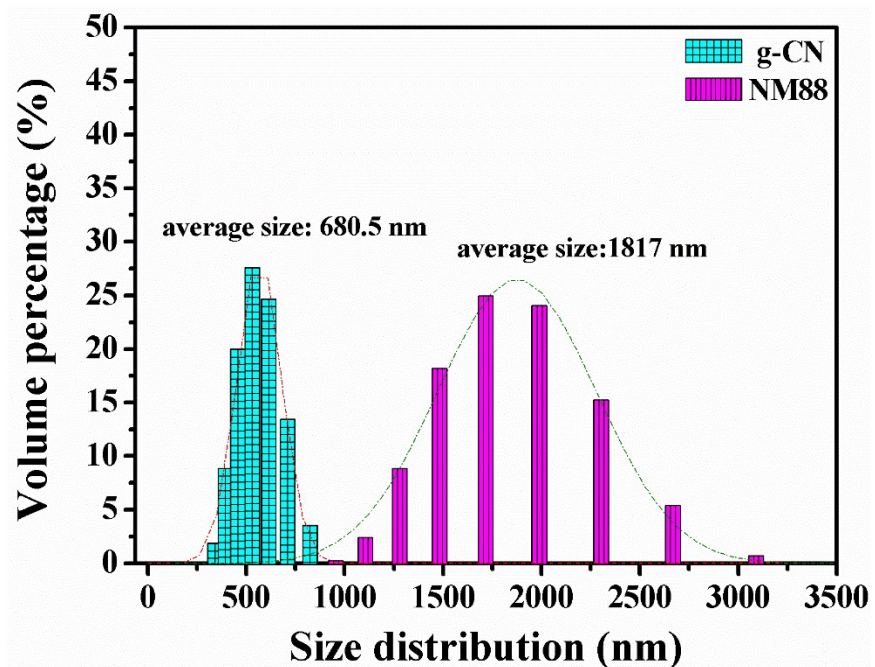


Figure S4. The size distribution of obtained materials.

Table S1. Specific surface area and porous texture information of the obtained materials

Properties	BET surface area (m ² /g)	Average pore Diameter (nm)	Pore volume (cm ³ /g)
BMFAs	52.06	5.59	0.07
g-CN	95.47	6.94	0.17
NM88	53.54	7.17	0.10
g-CN@NM88/BMFAs	24.33	6.52	0.04

Table S2. The volume density of BMFAs before and after modification

Properties	Mass (g)	Volume (cm ³)	Volume density (mg/cm ³)
BMFAs	0.2390	25.12	9.5
g-CN@NM88/BMFAs	0.5209	7.06	73.7



Figure S5. The photographs of BMFAs under different compression.

Table S3. The zeta potential information of the obtained materials under different pH values.

Properties	pH = 3.0	pH = 5.0	pH = 6.0	pH = 7.0	pH = 9.0
g-CN	23.8 ± 6.8	-9.3 ± 7.4	-14.0 ± 5.4	-17.4 ± 9.1	-20.9 ± 10.8
NM88	12.1 ± 4.0	-0.903 ± 4.87	-4.13 ± 4.94	-3.10 ± 4.56	-3.70 ± 4.74
Composite	14.5 ± 5.55	0.720 ± 5.55	-3.66 ± 3.83	-9.67 ± 4.51	-9.14 ± 5.21

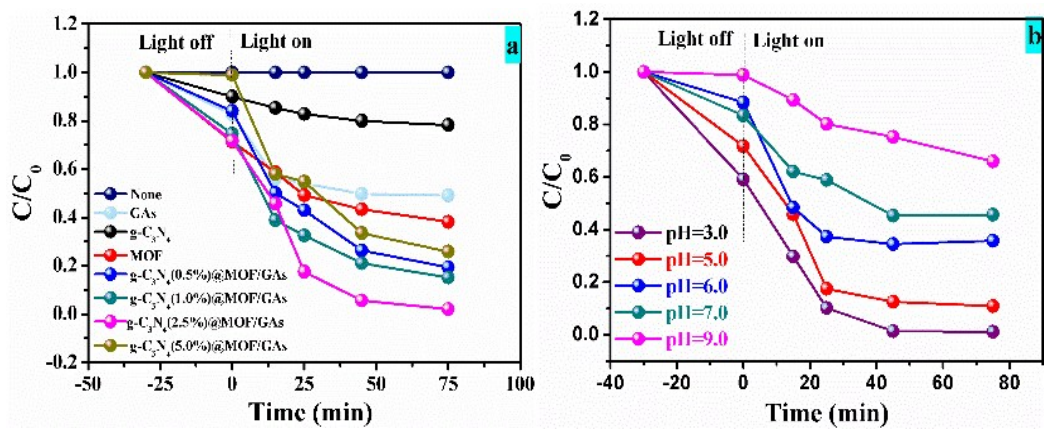


Figure S6. Photocatalytic activities of g-CN@NM88/BMFAs nanocomposite with various ratios towards Cr (VI) reduction (a) and effects of pH values (b).

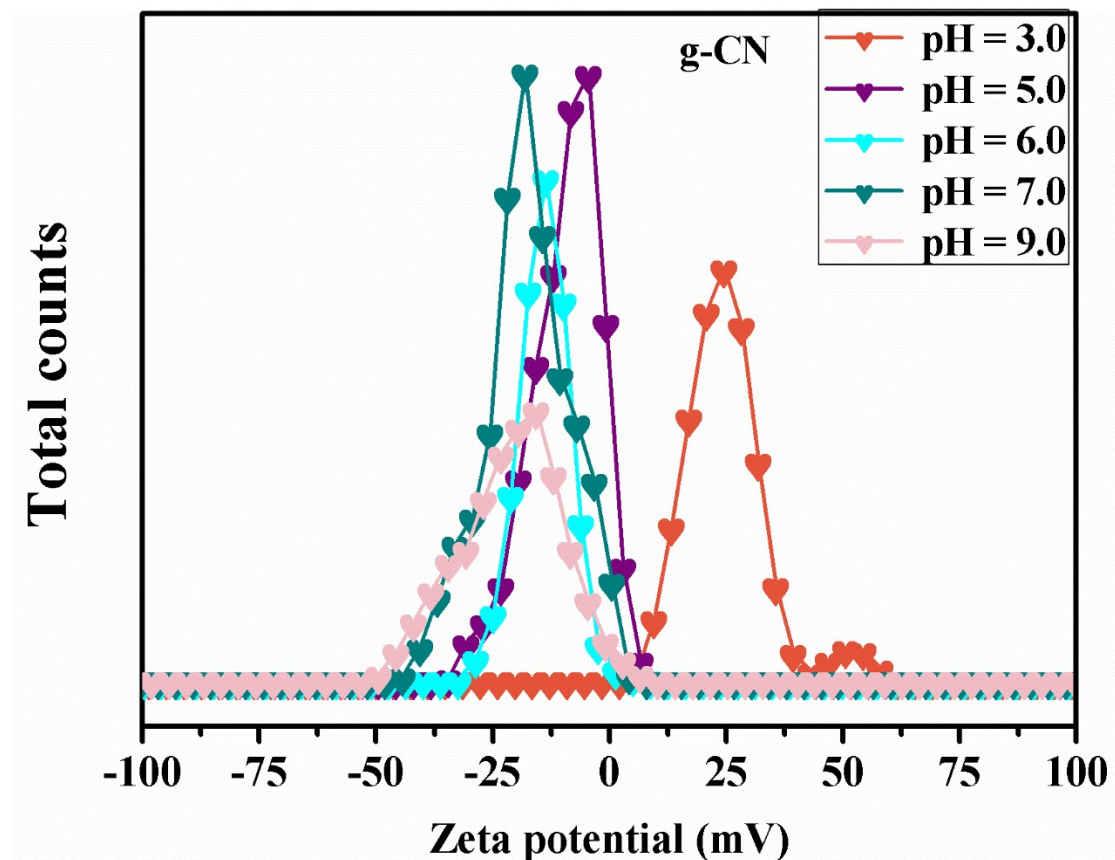


Figure S7. The zeta potential of g-CN under different pH values.

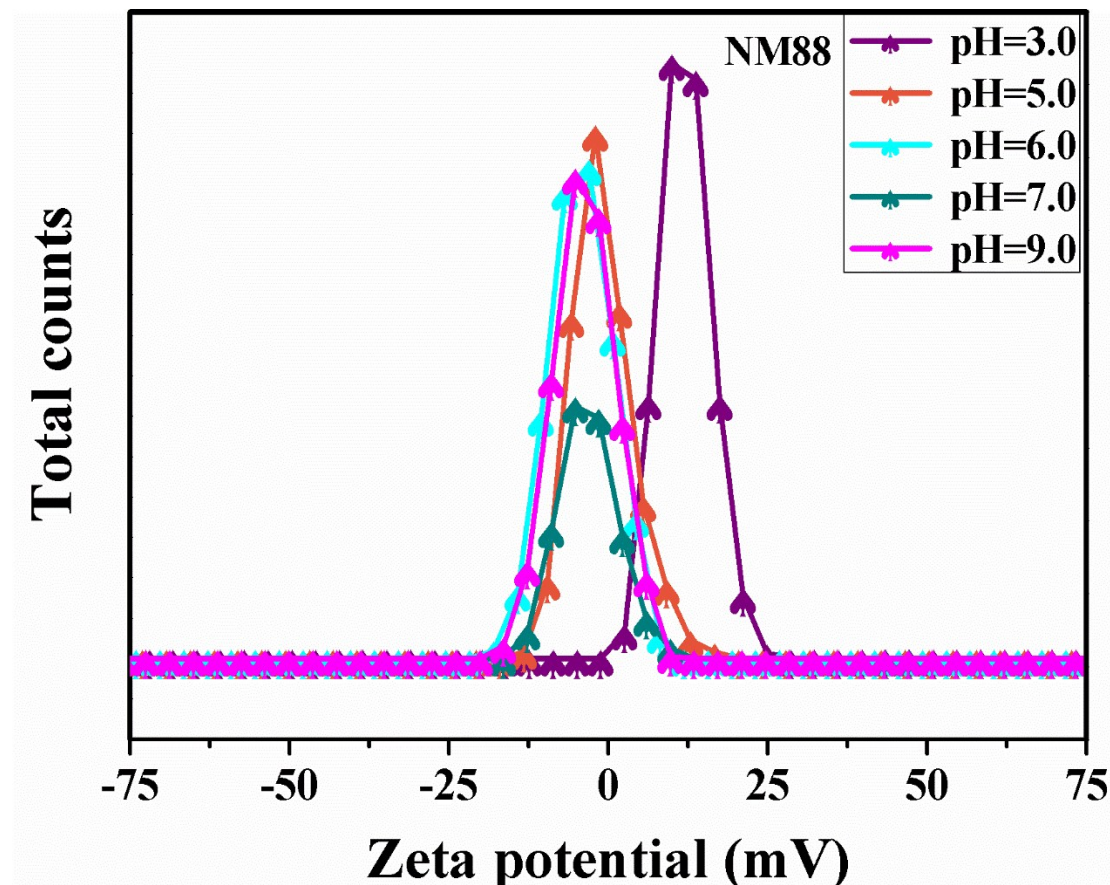


Figure S8. The zeta potential of NM88 under different pH values.

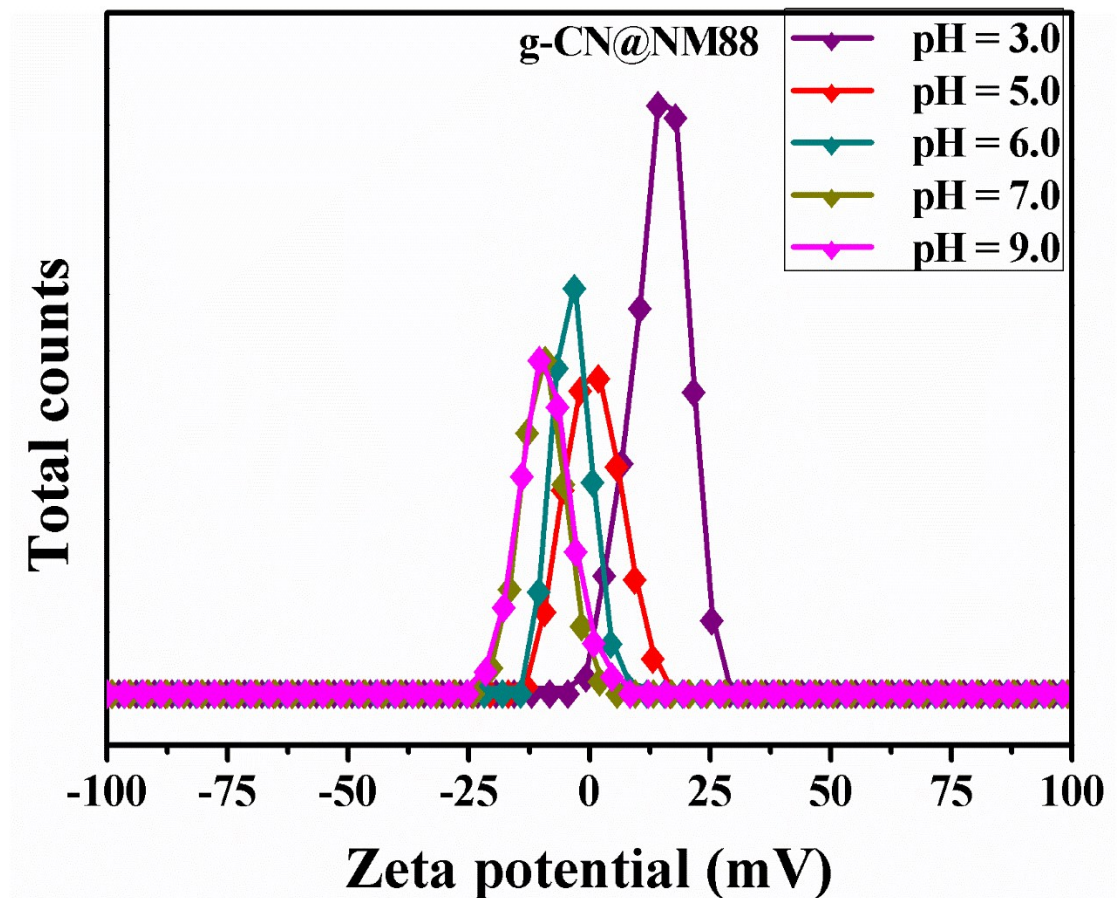


Figure S9. The zeta potential of g-CN@NM88 under different pH values.

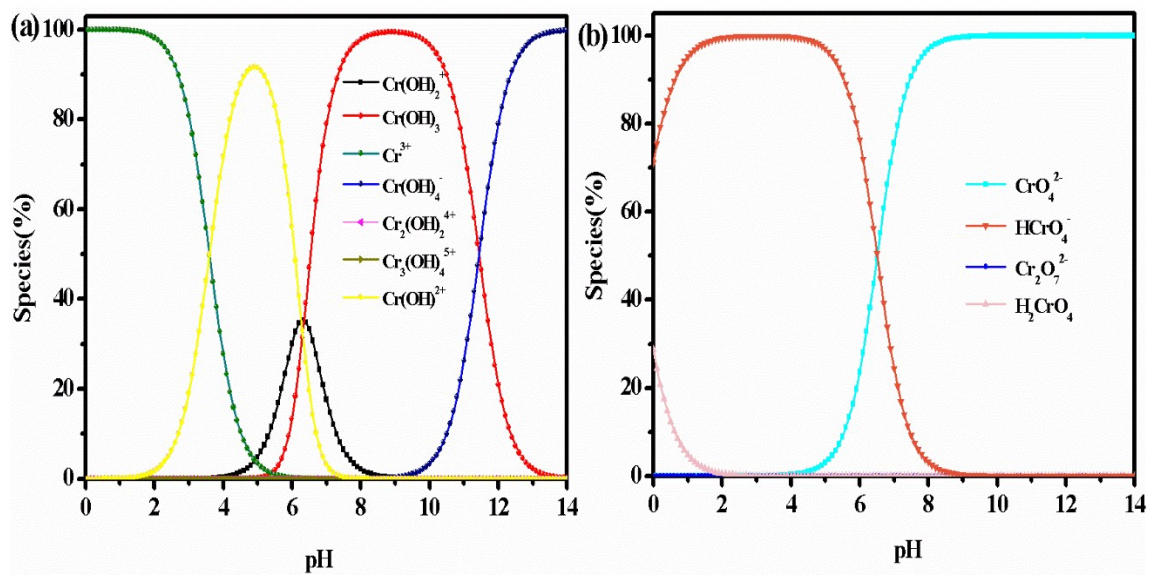


Figure S10. The species distribution of Cr (III) and Cr (VI) under different pH values.

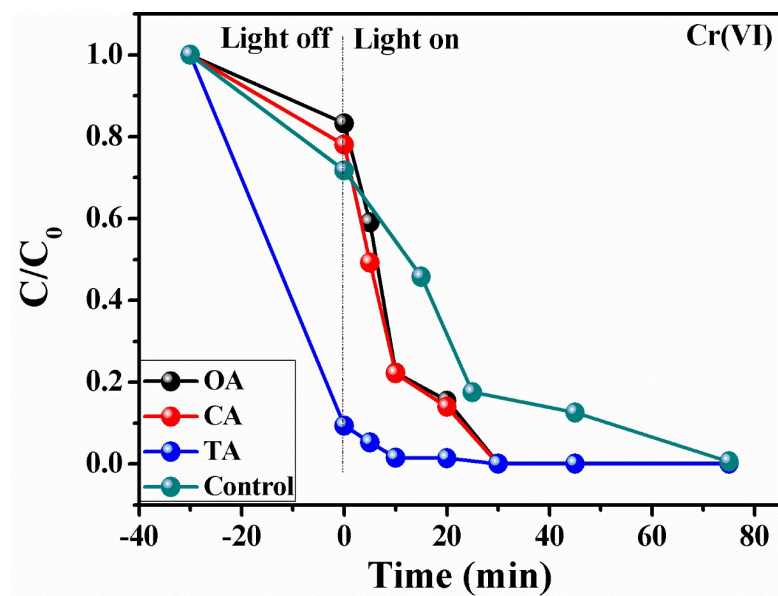


Figure S11. The effect of co-existing small molecular organic acids towards Cr (VI) reduction.

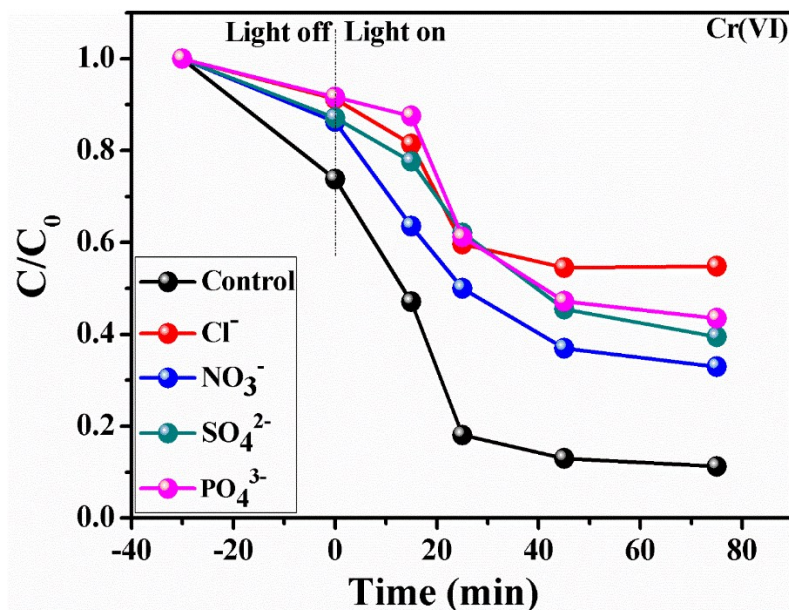


Figure S12. The effect of co-existing inorganic anions towards Cr (VI) reduction.

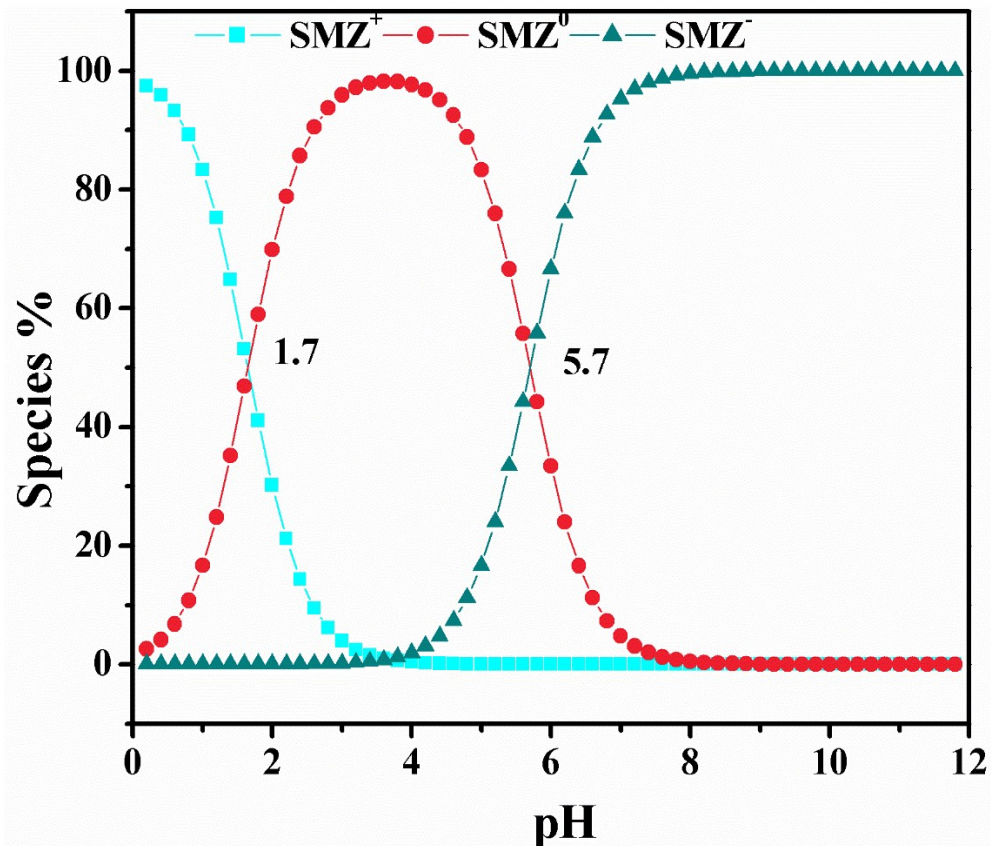


Figure S13. The species distribution of SMZ under different pH conditions.

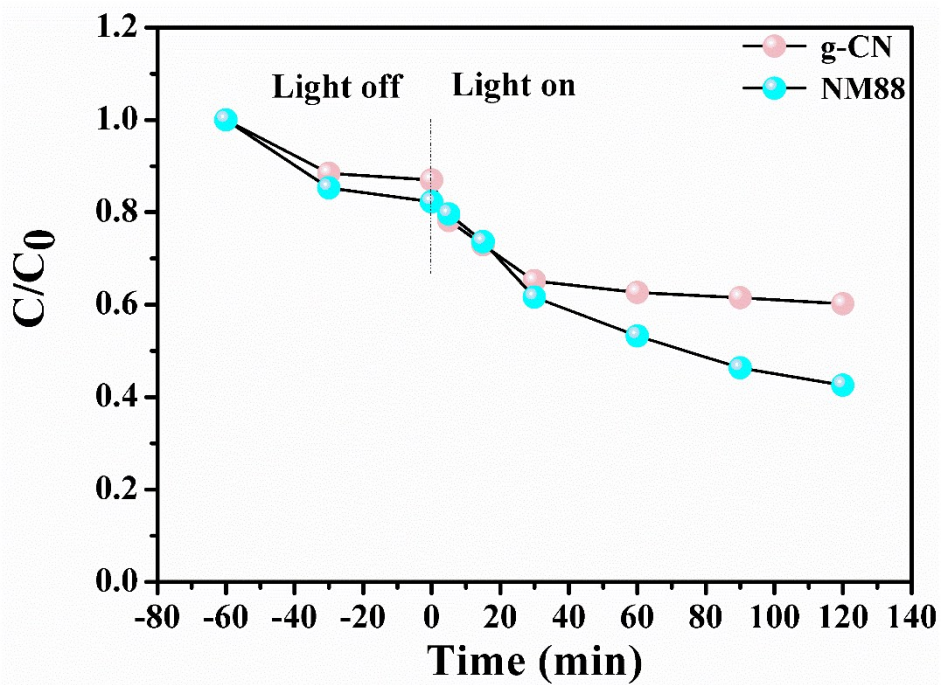


Figure S14. The degradation performance towards SMZ on g-CN and NM88.

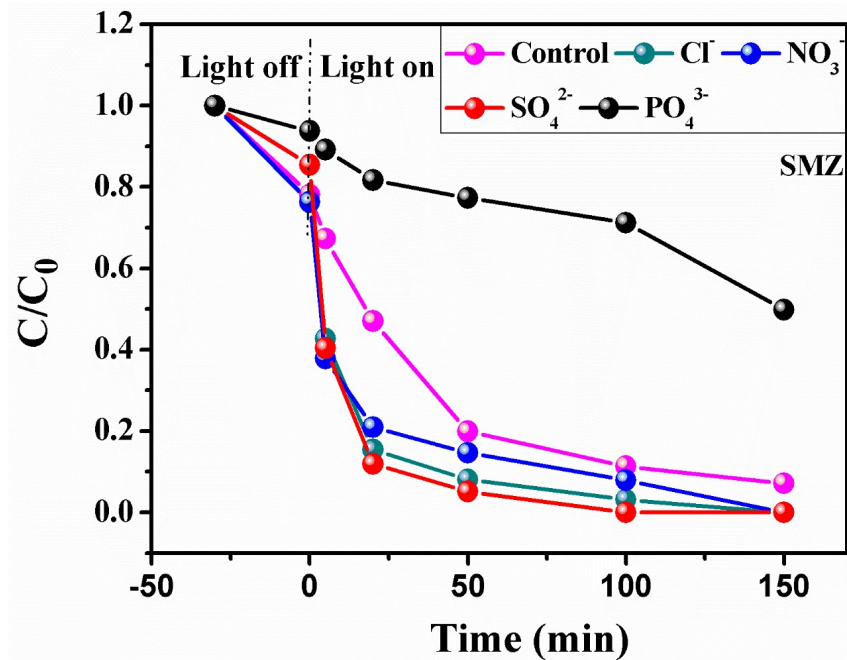


Figure S15. The effect of co-existing inorganic anions towards SMZ degradation.

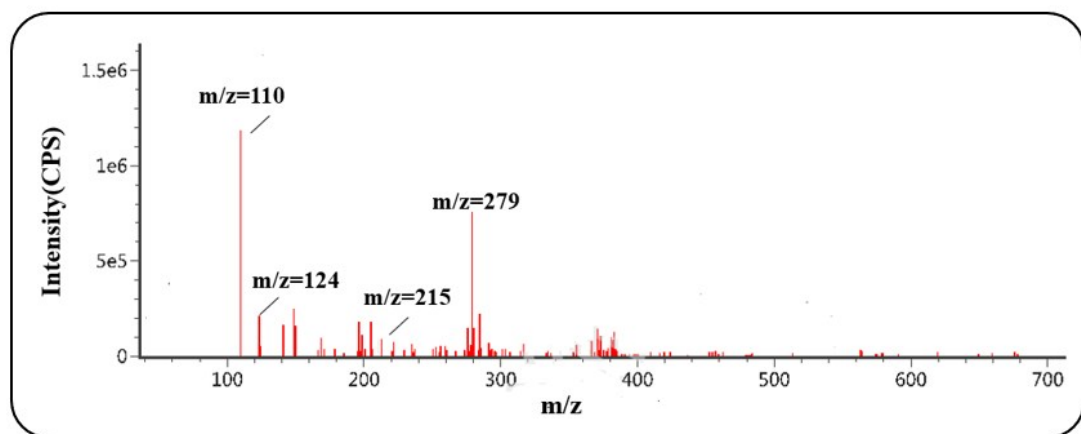


Figure S16. The mass spectrum for SMZ intermediates analysis.

Table S4. Comparison of hydrogen generation rate of the g-CN@NM88/BMFAs nanocomposite and other, previously reported materials

Materials	Hydrogen generation rate μmol g ⁻¹ h ⁻¹	Reference
Z-scheme g-C ₃ N ₄ /Ag/MoS ₂	104	1
g-C ₃ N ₄ /red phosphorous/MoS ₂	257.9	2
g-C ₃ N ₄ /WS ₂	101	3
(P, Mo)-g-C ₃ N _x	118	4
ZnO _{0.6} S _{0.4}	45.8	5
Ag bridged g-C ₃ N ₄ @WS ₂	686.2	6
2%Bi/g-C ₃ N ₄	718	7
Silicon carbide	198.1	8
CaIn ₂ S ₄ /g-C ₃ N ₄	102	9
g-CN@NM88/BMFAs nanocomposite	775	This work

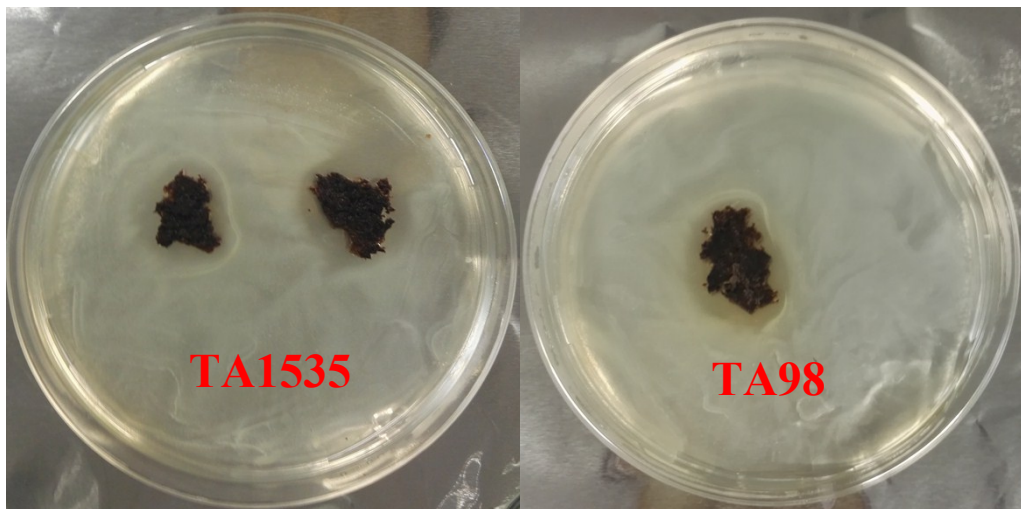


Figure S17. The antibacterial properties over g-CN@NM88/BMFAs nanocomposite for the salmonella typhimurium of TA1535 and TA98.

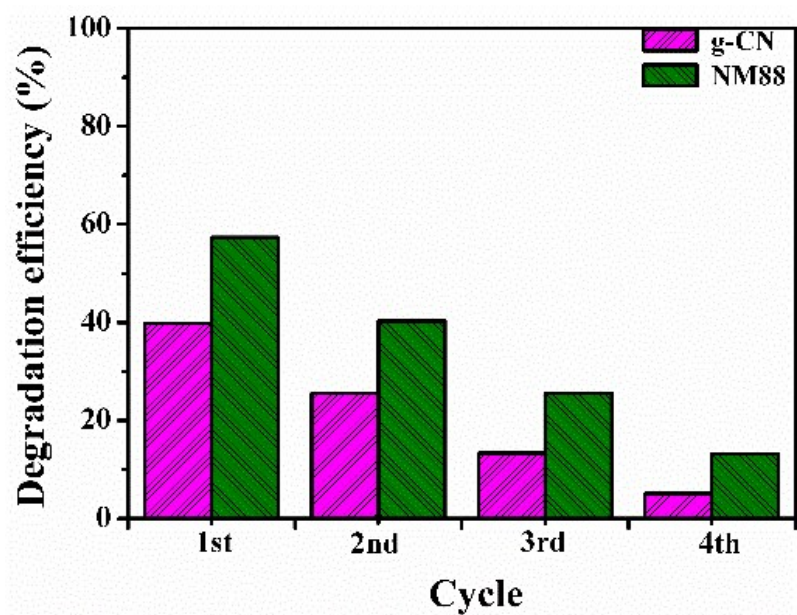


Figure S18. The stability of g-CN and NM88 for photocatalytic degradation of SMZ.

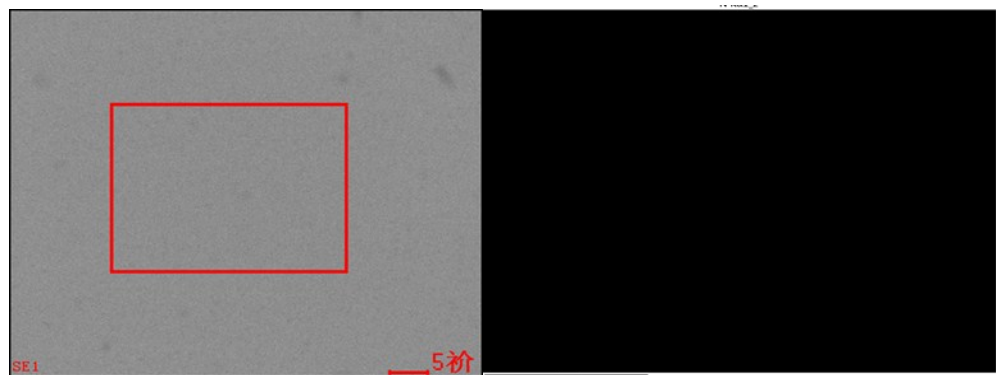


Figure S19. The SEM (Left) and EDS (Right) images of g-CN released to the reaction solution.

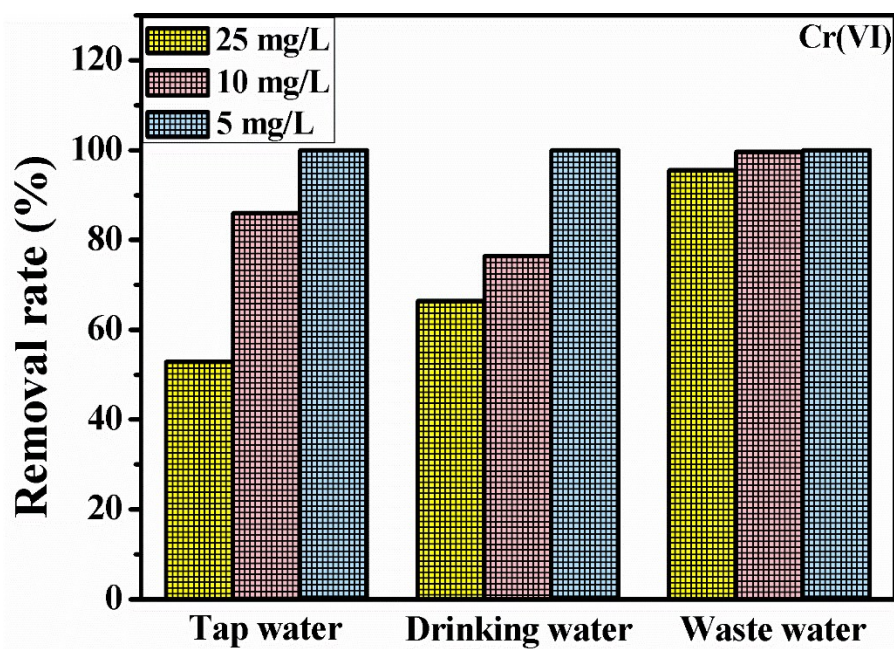


Figure S20. The removal efficiency for Cr (VI) by g-CN@NM88/BMFAs in different water sources.

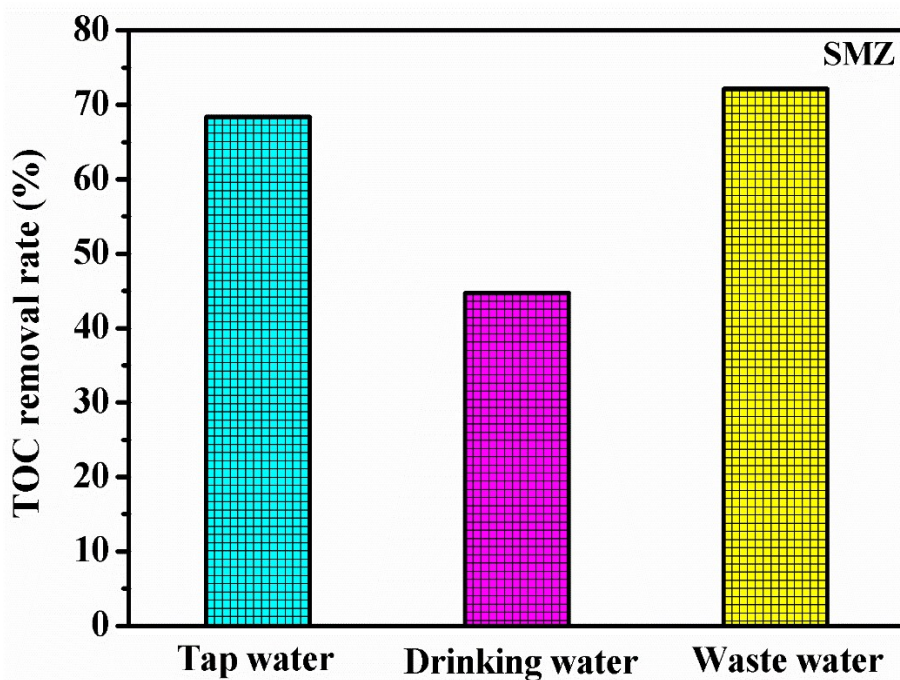


Figure S21 The TOC removal efficiency for SMZ by g-CN@NM88/BMFAs in different water sources.

References

1. J. Li, Y. Yin, E. Liu, Y. Ma, J. Wan, J. Fan and X. Hu, *J. Hazard. Mater.*, 2017, 321, 183–192.
2. J. Chen, D. Zhao, Z. Diao, M. Wang, L. Guo and S. Shen, *ACS Appl. Mater. Interfaces*, 2015, 7, 18843–18848.
3. R. Ye, H. Fang, Y. Z. Zheng, N. Li, Y. Wang and X. Tao, *ACS Appl. Mater. Interfaces*, 2016, 8, 13879–13889.
4. D. D. Chen, J. G. Liu, Z. Z. Jia, J. Z. Fang, F. Yang, Y. M. Tang, K. Wu, Z. Liu and Z. Q. Fang, *J. Hazard. Mater.*, 2019, 361, 294-304.
5. K. H. Chu, L. Ye, W. Wang, D. Wu, D. K. L. Chan, C. Zeng, H. Y. Yip, J. C. Yu and P. K. Wong, *Chemosphere*, 2017, 183, 219-228.
6. Y. N. Ma, J. Li, E. Z. Liu, J. Wan, X. Y. Hu and J. Fan, *Appl. Catal., B*, 2017, 219, 467-478.
7. Z. D. Wei, J. Y. Liu, W. J. Fang, M. Q. Xu, Z. Qin, Z. Jiang and W. F. Shangguan, *Chem. Eng. J.*, 2019, 358, 944-954.
8. Y. Zhang, Y. Hu, H. M. Zeng, L. Zhong, K. W. Liu, H. M. Cao, W. Li and H. J. Yan, *J. Hazard. Mater.*, 2017, 329, 22-29.
9. X. Yue, S. Yi, R. Wang, Z. Zhang and S. Qiu, *Sci. Rep.*, 2016, 6, 22268.